Wangzhong Mu*, Pär Göran Jönsson and Keiji Nakajima*

Recent Aspects on the Effect of Inclusion Characteristics on the Intragranular Ferrite Formation in Low Alloy Steels: A Review

DOI 10.1515/htmp-2016-0175
Received August 14, 2016; accepted February 2, 2017

Abstract: Intragranular ferrite (IGF), which nucleates from specific inclusion surfaces in low alloy steels, is the desired microstructure to improve mechanical properties of steel such as the toughness. This microstructure is especially important in the coarse grain heat affected zone (CGHAZ) of weldments. The latest review paper focusing on the role of non-metallic inclusions in the IGF formation in steels has been reported by Sarma et al. in 2009 (ISIJ int., 49(2009), 1063–1074). In recent years, large amount of papers have been presented to investigate different issues of this topic. This paper mainly highlights the frontiers of experimental and theoretical investigations on the effects of inclusion characteristics, such as the composition, size distribution and number density, on the IGF formation in low carbon low-alloyed steels, undertaken by the group of Applied Process Metallurgy, KTH Royal Institute of Technology. Related results reported in previous studies are also introduced. Also, plausible future work regarding various items of IGF formation is mentioned in each section. This work aims to give a better control of improving the steel quality during casting and in the heat affected zone (HAZ) of weldment, according to the concept of oxide metallurgy.

Keywords: inclusion, intragranular ferrite (IGF), nucleation, growth, steel, oxide metallurgy

***Corresponding authors: Wangzhong Mu,** McMaster Steel Research Centre, Department of Materials Science and Engineering, McMaster University, 1280 Main Street West, Hamilton, Ontario, Canada L8S 4L7; Formerly, Department of Materials Science and Engineering, KTH Royal Institute of Technology, Brinellvägen 23, SE-10044 Stockholm, Sweden, E-mail: wangzhongmu@gmail.com
Keiji Nakajima, Department of Materials Science and Engineering, KTH Royal Institute of Technology, Brinellvägen 23, SE-10044 Stockholm, Sweden, E-mail: keiji@kth.se
Pär Göran Jönsson, Department of Materials Science and Engineering, KTH Royal Institute of Technology, Brinellvägen 23, SE-10044 Stockholm, Sweden

Introduction

It is known that non-metallic inclusions in steels are considered to be detrimental for the mechanical properties. However, certain kinds of non-metallic inclusions may serve as potent nucleation sites for intragranular ferrite (IGF) formation in low carbon low alloy steels. When IGF nucleates from the inclusion surface, the formation of grain boundary ferrite (GBF) is suppressed. This phenomenon is based on the concept of oxide metallurgy [1–4]. Thus, this concept could be applied to improve the toughness and strength of coarse grains in the heat affected zone (CGHAZ) of weld metals. The schematic illustration of IGF formation in CGHAZ is shown in Figure 1. Specifically, the formation of IGF includes two kinetic process, its nucleation and growth. Moreover, it is apparent that the yield strength increases and the fracture appearance transition temperature decreases significantly with the increasing proportion of IGF [5–7].

Since the oxide metallurgy concept was provided in 1990, review papers focusing on IGF formation started to be published in around 2004, according to the authors' knowledge. Babu summarized several mechanisms of IGF formation in weldments [5]. Thereafter, Koseki and Thewlis provided a more comprehensive review on the inclusion assisted microstructure control in low alloy steel welds [6]. In their review paper, IGF transformation kinetics, effective inclusions for IGF formation, mechanisms of IGF nucleation and weldment properties have been summarized. The above reviews mainly focused on the weldment. Alternatively, the latest review focusing on the roles of non-metallic inclusions on IGF formation has been reported by Sarma et al. in 2009 [7]. Based on these previous reviews, the present work aims to highlight the frontiers of experimental and theoretical investigations on the formation of IGF during the austenite decomposition process, undertaken at the group of applied process metallurgy, KTH Royal Institute of Technology [8–16]. Related results reported in previous studies are also summarized. The novel steel sample preparation methods with ceramic particle additions, effects of inclusion compositions, size distributions and number densities on the IGF formation, modified model of IGF nucleation and in-situ

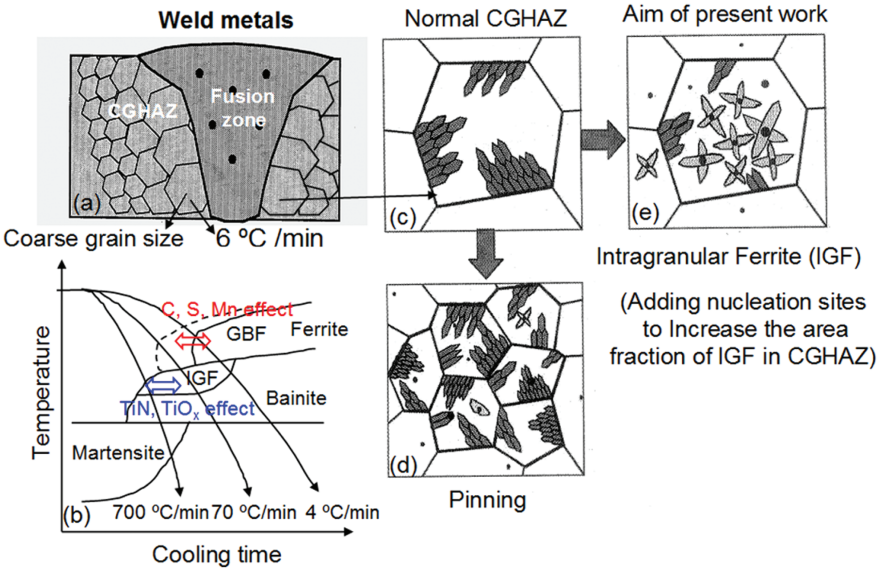

Figure 1: Schematic illustrations of (a) coarse grain heat affected zone (CGHZA), (b) CCT diagram, (c) GBF formation in CGHAZ, (d) pinning effect in CGHAZ and (e) IGF formation in CGHAZ.

observation of IGF formation using confocal laser scanning microscope (CLSM) are summarized. This work aims to give a better understanding of the correlation between inclusions and the microstructure according to the concept of oxide metallurgy.

Development of steel sample preparation methodology with pure ceramic particle additions

Normally, oxide inclusions formed in de-oxidation process are used as nucleation sites for IGF formation in steels. Different single and/or complex deoxidizing elements, such as Al, Ti, Mg, Zr, and rare earth can be selected. However, special designed steel alloys with pure ceramic particles additions are used to investigate potency of different nucleation sites to induce IGF formation. According to the authors' knowledge, prior work focusing on this subject is reported by Gregg and Bhadeshia [17]. They used two steel rods to first provide sandwich ceramic powders and then to hot pressed them at 1200 °C for 10 min. It was reported that this condition was sufficient to cause the ceramic and steel phases to bond together. Thereafter, the bonded specimens were sectioned in a plane normal to that of the ceramic/steel interface [17]. A schematic illustration is given in Figure 2(a). Subsequently, the method used by Zhang et al. [18] is quite similar to the sintering method reported by Gregg and Bhadeshia [17]. The only difference is that they put disc-shaped ceramic polycrystals between the steel cylinders in a small chamber, as illustrated in Figure 2(b).

Recently, Kasai et al. [19] and Lee et al. [20] reported on a newly developed method to insert single crystal TiO and TiN particles between steel rods and then hot press them at austenite temperatures. Thereafter, the specimens were reheated at 1050 °C and were held at this temperature for 25 min to accomplish the austenite grain growth. This is illustrated in Figure 2(c). By using this method, it was found that the single crystalline grains of TiO and TiN particles were embedded inside the austenite grains. Subsequently, the specimen was cooled down to different temperatures between 800 and 500 °C. To compare with previous sintering methods, the benefit of this method is that the formation of IGF could be observed from single ceramic particles of different sizes. Moreover, the single crystal particles were selected so that the crystal orientation relationship between the ferrite (BCC structure) and TiN and TiO particles (FCC structure) could be detected by using electron backscatter diffraction (EBSD).

The sintering method is a good methodology for fundamental studies of the mechanisms of IGF formation from different nucleation sites. One advantage is that nitride particles do not dissolve in steel matrix at a temperature less than 1200 °C. Also, the particle size changes on slightly in the bonding interface before and after sintering. However, there are difficulties in relating the results of as-sintered steel to the case of the actual steel solidified from liquid state. This is due to that the sintering methods do not necessarily lead to an intimate bond on atomic scale between the ceramic and steel interface.

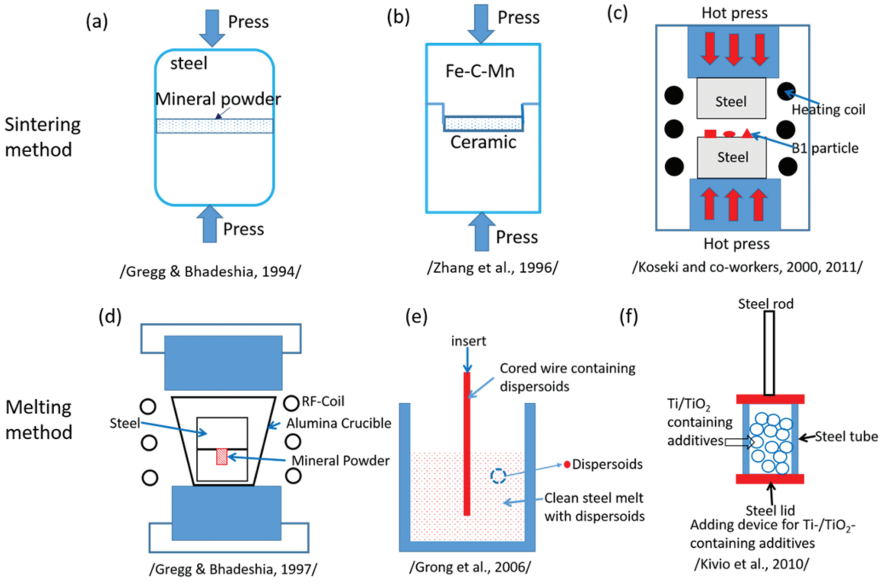

Figure 2: Schematic illustrations of different methods to prepare steels with pure ceramic powders additions, revised by the original figures in Refs [17–23].

If the steel matrix is melted, this disadvantage is not needed to be considered.

Prior work of the melting method by adding pure particles into steel is also made by Gregg and Bhadeshia [21]. They drilled a hollow on the cross section of a steel cylinder. Thereafter, they added ceramic powders into this hollow, melted the steel, held in the molten state for 5 seconds and subsequently cooled it. This procedure is schematically illustrated in Figure 2(d). Also, Grong et al. [22] provided an idea to add a cored wire containing a high number density of dispersoids to clean the steel melt, as illustrated in Figure 2(e). Another method based on this idea has been adopted by Kivio et al. [23]. They reported a new device which was used to add Ti/TiO_2, as shown in Figure 2(f). This device was placed into the middle of the mold inside the furnace chamber. During casting, the steel tube melted, and the Ti/TiO_2-containing additives were distributed into the liquid steel in the mold. They reported that grain refinement could be observed clearly. However, the presence of IGF could not be confirmed definitely after heat treatment of the solidified steel.

In very recent work, another method of preparing steels with pure ceramic powders additions has been reported by the authors [8, 9]. The schematic illustration is shown in Figure 3. Metallic powders in combination with graphite powder, FeS powder and ceramic powders including $TiN/Ti_2O_3/TiO_2$ were mixed together in a planetary ball mill. Thereafter, FeS powders were added to control the sulfur contents in the final steel sample. Different ceramic powders were used for each steel sample to act as nucleation sites of IGF formation. The mixed

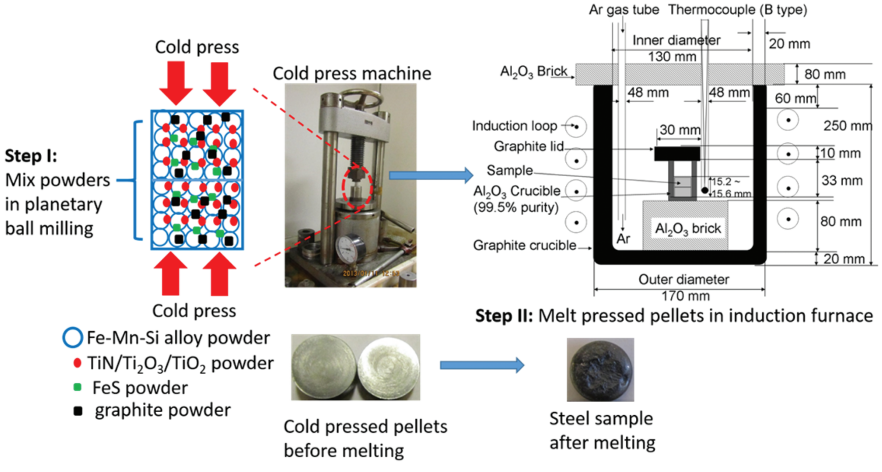

Figure 3: Schematic illustration of preparation method pf steel sample with TiN and Ti-oxides additions. This work is done by the present authors.

powders were cold-pressed into disk shaped pellets. Thereafter, the cold-pressed pellets were put in an Al_2O_3 crucible and were melted, held in the molten state in a very short time and subsequently cooled in a medium-frequency heating furnace with the protection of a high purity Ar gas. A schematic view of the size and the cutting position of the ingot samples is shown in Figure 4. A typical microstructure in the cross section of the steel, and different morphologies of IGF which are acicular type and polygonal type, are also shown in Figure 4. Subsequently, the same method has been applied by Gao et al. [24] to add MgO and AlSi nanoparticles into steel to investigate the importance of $MgAl_2O_4$ nucleation site for IGF formation. Another method for adding pure particles into the liquid steel have been presented by Xuan et al. [16]. Electrolytic iron, various ferrous alloys, and pure metals (Ti, Al) were first melted. Thereafter, pellet packets or wire packets containing TiN and TiO_2 nanoparticles were added into the liquid metal.

Compared to sintering method, the reported melting method resembles the case of IGF formation in actual steel grades more closely. However, the melting method is still not a perfect simulation of the production conditions. First of all, pure single phase particles which are added into liquid steel are changed to complex phases. This is caused by reactions between particles and alloying elements in steel. This has been found in all previous studies [8, 9, 14, 21–24]. Secondly, the size distribution of pure particles changes after addition into liquid steel, as reported in Refs [8, 9, 14]. An example of size distribution of Ti_2O_3 particles before and after adding into steels is shown in Figure 5 [15, 16]. Thirdly, nitride particles such as TiN and VN dissolve in liquid steel, and precipitate either on the grain boundary or on the surface of oxide inclusion during cooling [8]. The authors will work on developing a modified methodology to keep the phase and size distribution of pure particles in the whole steel bulk in the future.

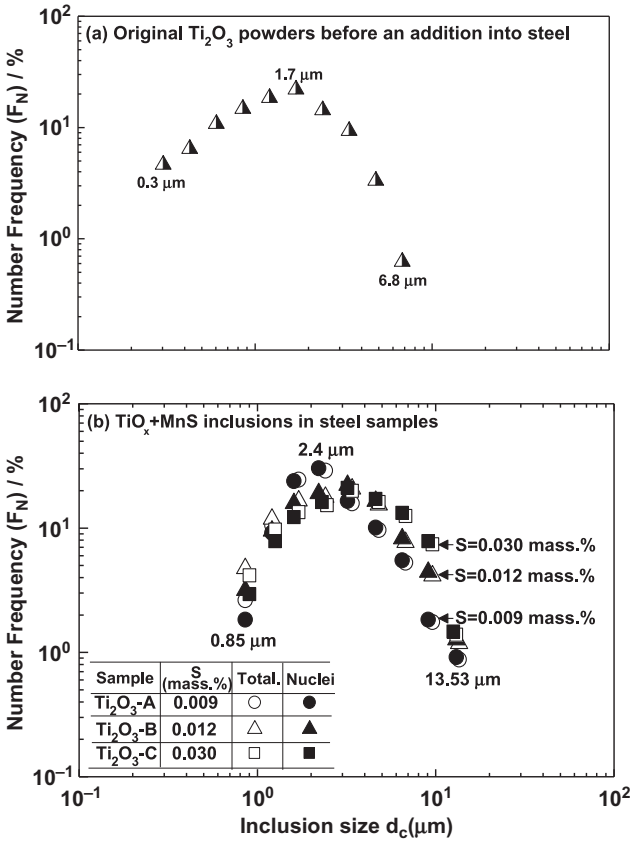

Figure 5: Size distribution of (a) original Ti_2O_3 powders and (b) TiO_x + MnS inclusions in steels with Ti_2O_3 additions [15, 16].

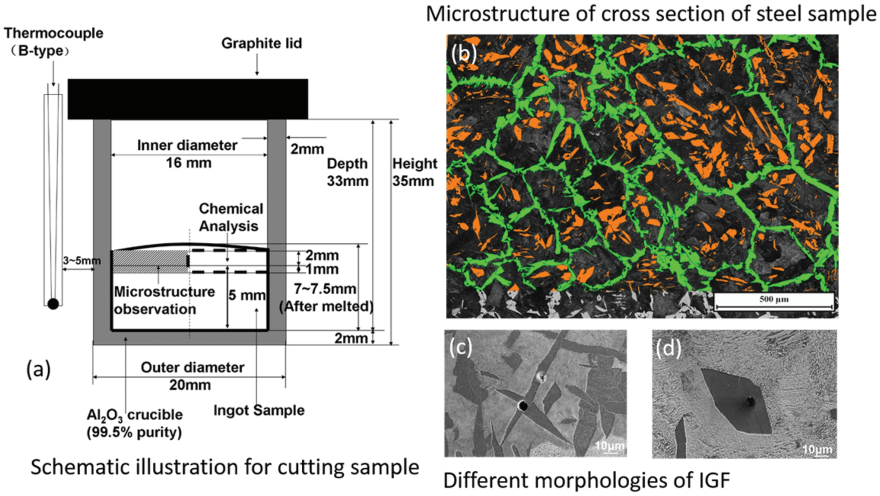

Figure 4: Illustrations of (a) cutting positions for microstructure observation and chemical analysis, (b) microstructure of cross section in the steel sample with TiN particles additions, and (c) and (d) different morphologies of IGF, reported by the present authors [8].

Parametric studies on the effect of the inclusion characteristics on IGF formation

Effect of inclusion composition

Whole composition of inclusion

Based on previous studies, a brief summary of the influence of chemical compositions of inclusions on IGF formation is described as below. Single oxides, such as Ti_2O_3 [25–28] and TiO [19, 20, 29, 30], single nitrides, such as TiN [29–33] and VN [18, 34], single sulfides, such as CuS [35] and CeS [36], galaxite spinel ($MnO•Al_2O_3$) [36] and multi-phase inclusions, such as TiN + MnS [37–39], Ti_2O_3 + TiN [39], TiN + Ti_2O_3 + MnS [40], TiN + MnS + $Fe_{23}(CB)_6$ [41], V(C,N) + MnS [42, 43] and VC + MnS [42, 43] are reported to be the effective nucleation sites for IGF. On the other hand, other types of inclusions, such as Al_2O_3 [21, 34], SiO_2 [34, 44], MnS [21, 34, 42, 43] and $MnO•SiO_2$ [27, 34] are not potent nucleation sites.

In recent years, Zr-containing complex inclusions, which have been seldom discussed in the open literatures, are considered to be effective nucleation sites for IGF. Guo et al. [44] and Shi et al. [45] reported that complex ZrO_2 + MnS inclusions can induce IGF formation in HSLA pipeline steels and Ti-Zr deoxidized micro-alloyed steels. Moreover, Ti, Zr-oxide [46], ZrO_2 + MnS + TiN [47], Zr-Ti-Si-Mn-O + MnS [48], Al-Mg-Zr-O [49] and Al-Mg-Zr-O + MnS [49] complex inclusions are subsequently reported to be potent for IGF formation. The mechanism of IGF formation from Zr-containing nucleation site was according to Li et al. [50] that a diffusion of Mn into ZrO_2 leads to the formation Mn-depleted zone in the vicinity of ZrO_2 inclusion. This viewpoint was supported by both experimental studies and first principle calculations. Besides, in-situ observation of IGF formation in 16 Mn steel has been reported. Specifically, Ce-oxysulfide and Ce-sulfide were identified as nucleation sites [51]. $MgO•Al_2O_3$ + MnS is also reported to be potent for IGF formation [52]. It might be reasonable because of the crystal structure of $MgO•Al_2O_3$. However, it is well known that $MgO•Al_2O_3$ can lead to serious problems of nozzle clogging during casting. In this case, the size of $MgO•Al_2O_3$ nucleation site should be controlled in a narrow range, to avoid this problem. According to the authors' view point, a complex $MgO•Al_2O_3$ inclusion is not a recommended nucleation site for IGF formation.

Surface composition of inclusion

Previous studies reported that several kinds of complex inclusions can be effective for IGF formation. However, the complex composition includes different parts of the total inclusion. The authors can emphasis that the whole composition has no meaning when considering the inclusion characteristics related to the IGF formation. Instead, the surface composition of the inclusion should be the focus in order to explain the mechanism of IGF formation.

In previous studies by the authors, the complex TiN + Mn-Ti-Al-Si-O + MnS inclusion is a typical inclusion in a low carbon steel with TiN addition [8]. Also, TiO_x + MnS with small amount of liquid oxide is the typical inclusion formed in the low carbon steels with Ti_2O_3 and TiO_2 additions [9]. Examples of element mapping by SEM-EDS are given in Figure 6(a) and (b) [8–10] and by EPMA in Figure 7(a) and (b) [11]. Actually, the effective nucleation site is TiN and TiO_x (x = 1.5–1.7) for the two cases, respectively. The viewpoint of the authors is that the surface of the inclusion where IGF originates is the actual nucleation site.

Based on previous studies [8, 9, 42], it was concluded that the potency order can be as follows: TiO_x (x = 1.5–1.7) >TiO_x + MnS > TiN + Mn-Si-Al-Ti-O + MnS > V(C,N) + MnS > VC + MnS. This tendency is based on the experimental results presented in Refs [8, 9, 42]. Also, MnS and liquid oxide (Mn-Al-Si-O) inclusions are not potent nucleation sites. If considering the surface of inclusion, the order can be as follows: TiO_x (x = 1.5–1.7) > TiN > V(C,N) > VC. This different potency is due to interfacial energies between the inclusion and ferrite/austenite. The details can be seen in Refs [8–16]. by the authors. In addition, it is reported that increasing sulfur content can decrease IGF nucleation potency at each inclusion size range [8, 9]. This is because a larger amount of MnS forms, which covers the surface of the effective nuclei interface. Details are given in in Refs [8, 9]. Based the development of the characterization methodology, future work can focus on the interface of nuclei inclusion where IGF originates, in order to investigate different potencies of different nucleation sites.

In future work, the influence of composite precipitates containing Nb, V and Ti on the influence of surface composition of inclusion should be studied. The Nb-rich precipitate, specifically NbC and Nb(C,N), hold the same NaCl type crystal structure as TiN and VN. Moreover, the interfacial energy between NbC/NbN and austenite/ferrite is similar in the case of TiN and VN, as reported by Yang et al. [53]. Since TiN, VN and V(C,N) are well known

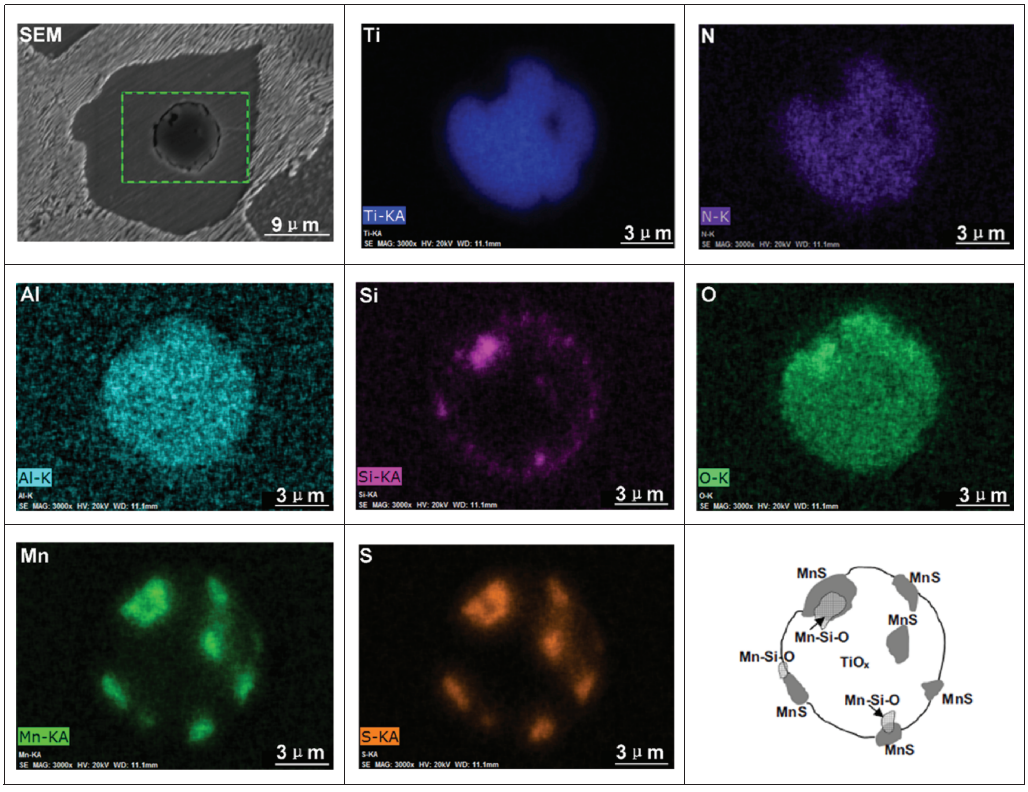

(a)

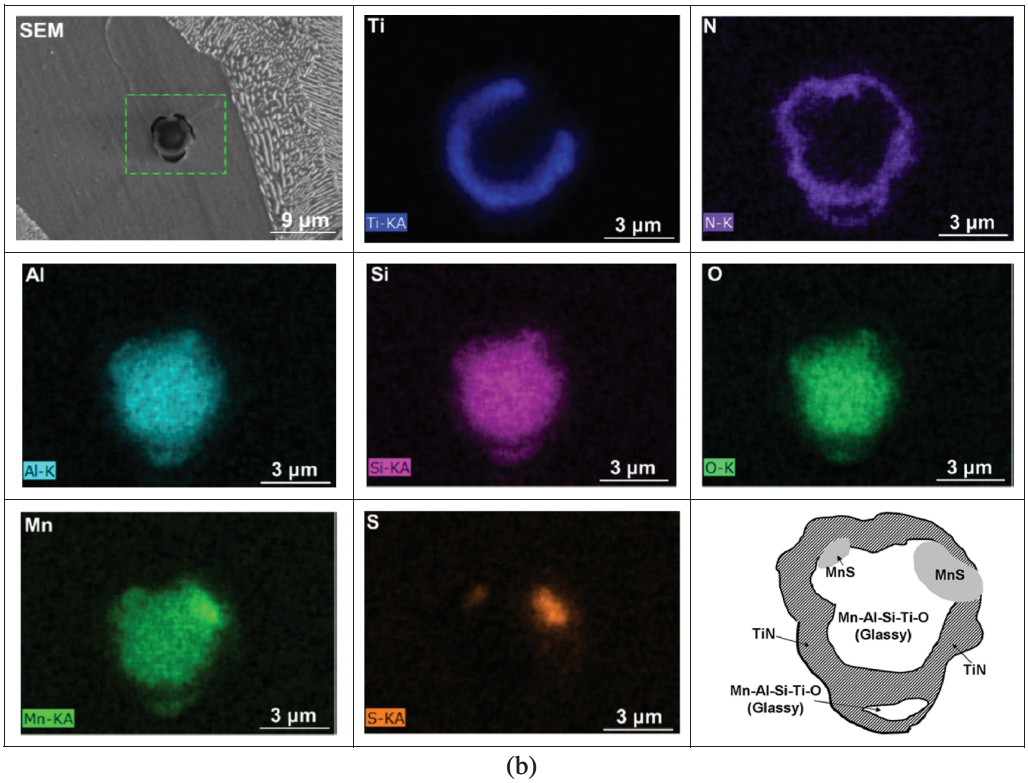

(b)

Figure 6: SEM micrographs and element mapping images of typical inclusions in (a) steel with Ti_2O_3 addition and (b) steel with TiN addition [8–10].

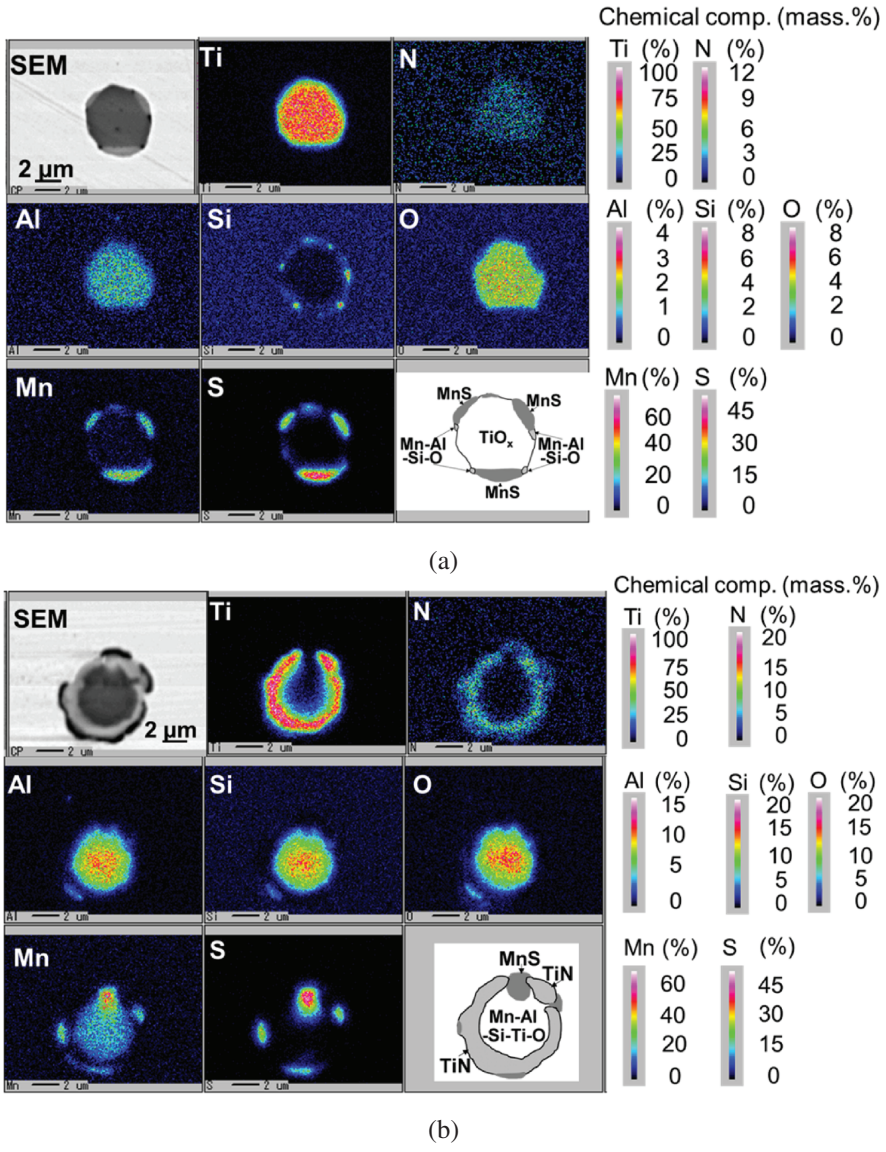

Figure 7: Element maps of Ti, N, Al, Si, O, Mn and S in inclusions of (a) steel with Ti_2O_3 addition and (b) steel with TiN addition, determined by EPMA [11].

effective nucleation sites for IGF [18, 29–34, 42, 43], NbC/NbN/Nb(C,N) has the theoretical potency to act as a nucleation site. It has been reported that homogeneously distributed composite precipitates such as (V, Ti)(C, N) [54], (Ti, Nb)C [55, 56] and (Ti, Nb)(C, N) [56, 57] with nanoscale sizes can enhance steel mechanical properties such as the toughness and strength. However, composite precipitates with the size of several micrometers, especially Nb-rich precipitates on the surface of inclusion have not been widely reported to act as nucleation sites for IGF. This can be considered in future work. Moreover, the authors use the composition of Ti and Nb microalloyed steel from Ref. [58]. to predict inclusion precipitation in thermodynamics using the Thermo-Calc with TCFE7 database [59]. The result is shown in Figure 8. The details of this prediction method are given in Refs [8, 9, 13]. Specifically, it is reported that this method can predict the existence of a precipitation phase in solid steel. Figure 8 shows that both Nb(C,N) and TiN exist in the solid steel, and Nb(C,N) precipitates at a lower temperature than TiN forms. This calculation result fits the experimental evidence reported in Ref. [57]. The different precipitation temperature can be applied to control the size and formation of each phase precipitate.

As a summary, it seems that MO_x, MN and MC with NaCl structure are recommended as suitable surface

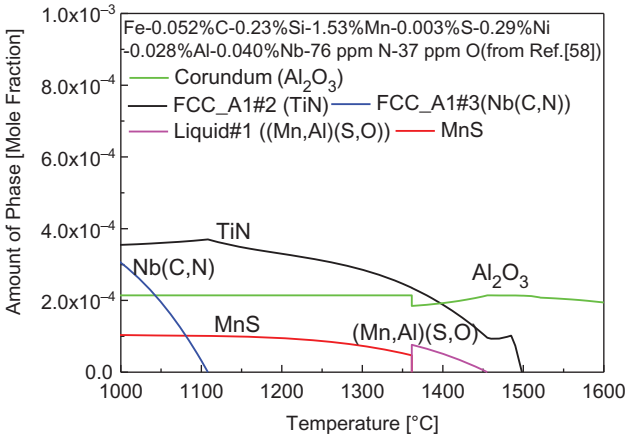

Figure 8: Thermodynamic calculation of inclusion precipitate using the composition of Nb, Ti micro-alloyed steel from Ref. [58].

compositions of inclusion to induce IGF formation. Here, M represents the elements in IVB group such as Ti and Zr, and VB group such as V and Nb. In order to control the surface composition of inclusion, the authors can recommend that the less Al deoxidation process in a liquid state for obtaining suitable oxide formation (MO_x), and the consequent precipitation process for obtaining nitride (MN) and carbide (MC) during cooling. In this case, equilibrium calculation by using thermodynamic calculation software, such as Thermo-Calc, is very useful to predict the inclusion formation in actual multi-component steel.

Effect of inclusion size

Besides the inclusion composition, the inclusion size also affects the potency of IGF formation. Table 1 summarizes previous experimental studies of effective inclusion sizes for IGF formation. Grong et al. [22] suggested that the size of nuclei inclusion should be strictly controlled to have values around 1 µm. Specifically, St-Laurent and L'Espérance [60] reported that the critical diameter of TiO for IGF formation was 0.45 µm. Similarly, Zhang and Farrar [61] reported that the most favorable inclusion size of Ti-rich oxide (probably TiO) inclusion was 0.3–0.9 µm for weld metals with intermediate oxygen contents (200–350 ppm), and 0.35–0.75 µm for weld metals with low oxygen contents (15–30 ppm). Hajeri et al. [62] found that the most effective size of Ti-oxide was above 2.0 µm. Besides the case of Ti-rich oxide, Li et al. [50, 58] and Min et al. [52] reported that the effective inclusion size for IGF formation is 1.5–3.0 µm for Al_2O_3-MgO-MnS inclusions, 1.5–2.0 µm for Al_2O_3-MgO-ZrO_2 inclusions and 2.0–5.0 µm for Al_2O_3-MgO-ZrO_2-MnS inclusions. The effective inclusion size varies slightly according to the different steel compositions.

Several studies reported that the nucleation potency of IGF formation is systematically increased with increasing inclusion size [8, 9, 42, 63]. The summary of previous studies focusing on this topic is shown in Figure 9. The potency for IGF nucleation (P_i) of inclusion at each size d_i, was estimated by using the number of nuclei inclusions at each size range ($N_{nu,i}$) divided by total number of inclusions at each size range ($N_{total,i}$). The values of $N_{nu,i}$ and $N_{total,i}$ are based on the size distribution of nuclei as well as total inclusions. In Figure 9, it is found that the increased inclusions size markedly enhances the IGF nucleation potency. Furthermore, this tendency can be observed in all the experiment data of complex oxides containing Ti [63], TiN + Mn-Si-Al-Ti-O + MnS [8], TiO_x + MnS [9], V(C,N) + MnS [42] and VC + MnS [42].

Table 1: Summary of experimental studies of effective inclusion size for IGF nucleation.

Inclusion group		Inclusion type	Effective inclusion diameter [µm]	Ref.
	Ti-oxide	TiO	0.45	[60]
		Ti-rich oxide (probably TiO)	0.3–0.9 (200–350 ppm O)	[61]
			0.35–0.75 (15–30 ppm O)	
		Ti-oxide	>2.0	[62]
	Spinel containing Mg, Al, Zr	Al_2O_3-MgO-MnS	2.0–3.0 (6 ppm Mg, 50 ppm Zr in steel)	[50, 52, 58]
			1.5–2.0 (8 ppm Mg, 300 ppm Zr in steel)	
			1.5–2.5 (24 ppm Mg, 300 ppm Zr in steel)	
		Al_2O_3-MgO-ZrO_2	1.5–2.0 (6 ppm Mg, 50 ppm Zr in steel)	
		Al_2O_3-MgO-ZrO_2-MnS	2.0–3.0 (8 ppm Mg, 300 ppm Zr in steel)	
			4.0–5.0 (22 ppm Mg, 50 ppm Zr in steel)	
			2.5–3.0 (24 ppm Mg, 300 ppm Zr in steel)	
Nitride/ Carbonatite	TiN	TiN + Mn-Al-Si-Ti-O + MnS	<0.7	[8]
	V(C,N)	V(C,N) + MnS	<2	[42]

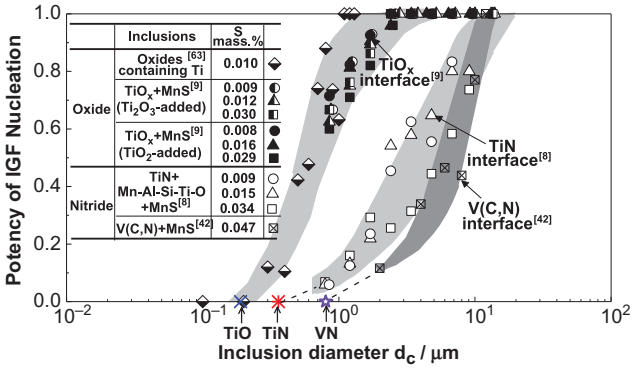

Figure 9: Summary of effect of nuclei inclusion size on IGF nucleation potency from Refs [8, 9, 42, 63].

However, it is well known that a very large size inclusion is detrimental for the mechanical prosperities of steels. In this case, both the IGF nucleation potency and the inclusion size should be considered to reach a high toughness of the steel.

From previous experiences, it is concluded that the suitable size of TiO inclusion for IGF formation ranged from 0.45 to 2.0 μm. The minimum size means the critical size of nucleation site for IGF, and the maximum size means the lower limit for "harmful". Of course the critical size of the nucleation site is a little bit changed due to the inclusion surface composition. The mechanism of this phenomenon will be quantitatively discussed in the following chapter. The peak position should be controlled from the critical size of nucleation site up to a size of 2.0 μm. In order to control this sub-micron size inclusion, a smaller Al content in the steel is needed to prevent a possible inclusion agglomeration. Besides, the critical size of more kinds of nuclei inclusions can be investigated in future work.

Effect of inclusion number density

In the work by the authors [8–16], the number density of nuclei inclusions were controlled to have almost the same values. This was done to investigate the effects of the inclusion compositions and inclusion sizes on IGF formation. However, it is considered that the increased inclusion number density can increase the area fraction of IGF. This is due to that a larger number of nucleation sites exist. This consideration has been confirmed in previous studies [64, 65]. Also, Oh et al. [64] reported that the number density of inclusions is more effective than size distribution of inclusions on IGF formation. Also, they reported that a higher oxygen and nitrogen contents lead to a higher number density of inclusions. However, a variation of the titanium content does not affect the number density of inclusions significantly. Similarly, Kim et al. [65] found that IGF was in proportion to the number density of inclusions which were smaller than 2 μm. Also, they reported that the average size of inclusions increased but their number density decreased with the increased heat input during submerged-arc-welding. Moreover, Kikuchi et al. [66–69] mentioned that oxide inclusion sizes in all the Ti-killed low-C high-Mn steels were smaller and that the inclusion densities were higher than those in Al-killed steels. In Ti-killed steels, the inclusion size and densities increased with increased the oxygen contents. Alternatively, the inclusion size decreased and their densities increased with increased cooling rates. In addition, they also found that IGF density increased with increasing number density of inclusions in steels.

In the future work on this subject, the key is how to get a high number density of nuclei inclusion with a narrow size distribution. In addition, the peak of this size distribution should be slightly larger than the critical size of nuclei for IGF formation. The schematic illustration of this idea in combination with a previous idea by Grong et al. [22] is shown in Figure 10. It is reported that the volume fraction of nuclei inclusion is only affected by impurity elements such as O and N, but it is not significantly affected by micro-alloying element such as Ti [64, 66–69], etc. In this case, the number density of nuclei inclusions should not be increased by controlling the steel composition in order to keep the cleanliness of

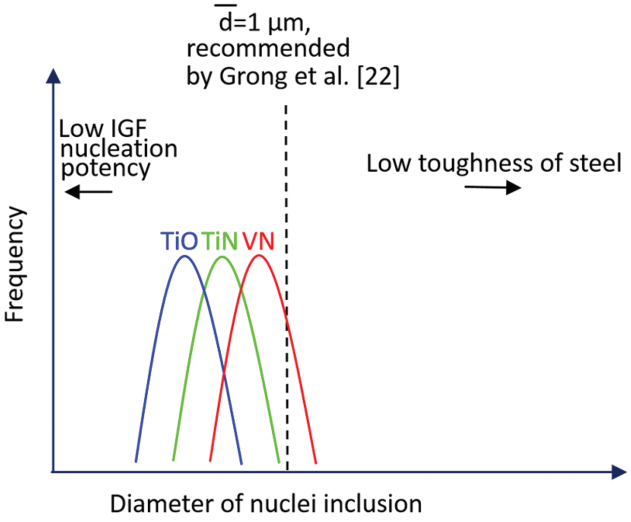

Figure 10: Schematic illustration of optimized size distribution of nuclei inclusions in steel.

steels. It is also important to control the cooling rate to decrease the inclusion size and to increase its number density, based on mass balance. It should be emphasized that the size of nuclei inclusion should not be too small, since IGF can only nucleate from the nuclei when its size is larger than the critical size.

Novel aspects on mechanism of IGF formation

Modified IGF nucleation model

According to the classical nucleation theory, the calculation methods for heterogeneous nucleation of ferrite from a spherical cap nucleation site have been reported in previous studies [70–72]. This nucleation is the initial stage of IGF formation. Also, Ricks et al. [73] and Byun et al. [74] have used this model to evaluate the energy barrier of ferrite nucleation from the grain boundary and from nuclei inclusions present inside grains. However, the energy barrier of IGF nucleation from different nucleation sites have not considered in previous models. Neither, IGF nucleation in steel matrix with the different compositions, such as: C and Mn cannot be evaluated.

Based on the limits of previous works, a modified model to predict IGF nucleation from a spherical shape nucleation site has been developed by the authors [10]. The contribution of this model is a quantitative evaluation of the energy barrier of IGF nucleation from different nucleation sites, based on the interfacial energies between nuclei inclusions and austenite/ferrite. Also, the effect of different element contents of the steel matrix on IGF nucleation can also be quantitatively investigated. The schematic geometry of IGF nucleation on a spherical inclusion surface is shown in Figure 11(a). In this image, the nuclei inclusion is simplified to have a spherical shape. In addition, the actual SEM image of IGF nucleated from the surface of the inclusion is shown in Figure 11(b). The details of this model are provided in Ref. [10]. The function between the normalized energy barrier for IGF nucleation, $\Delta G^*_{\text{het.}}/\Delta G^*_{\text{hom.}}$ and the inclusion size can be expressed as shown in eq. (1). The parameter θ represents the angle between the surface of the inclusion and the ferrite phase, as is illustrated in Figure 11(a). $\cos\theta$ is calculated by eq. (2), where, $\sigma_{I\alpha}$ is the interfacial energy between the inclusion and the ferrite, $\sigma_{I\gamma}$ is the interfacial energy between the inclusion and the austenite, and $\sigma_{\gamma\alpha}$ is the interfacial energy between the austenite and the ferrite. Furthermore, u and x are defined to simplify the expression of $f(\theta,x)$ as shown in eqs (3) and (4). Here, R is the radius of the inclusion, and r^* is the critical radius of the IGF, which can be calculated based on eq. (5). The parameter ΔG_v is the driving force for ferrite nucleation, calculated by Thermo-Calc.

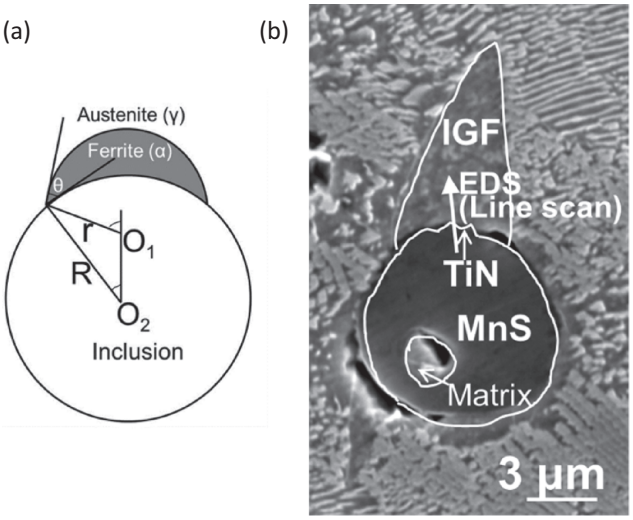

Figure 11: (a) Schematic geometry and (b) SEM observation of IGF nucleation on a spherical cap nuclei inclusion [10].

$$f(\theta,x)=\Delta G^*_{\text{het}}/\Delta G^*_{\text{hom}} = \frac{1}{2}+\frac{1}{2}\left(\frac{1-x\cos\theta}{u}\right)^3+\frac{x^3}{2}\left(2-3\left(\frac{x-\cos\theta}{u}\right)+\left(\frac{x-\cos\theta}{u}\right)^3\right)+\frac{3x^2\cos\theta}{2}\left(\frac{x-\cos\theta}{u}-1\right) \quad (1)$$

$$\cos\theta=(\sigma_{I\gamma}-\sigma_{I\alpha})/\sigma_{\gamma\alpha} \quad (2)$$

$$u=(1+x^2-2x\cos\theta)^{1/2} \quad (3)$$

$$x=R/r^*=R/(2\sigma_{\gamma\alpha}/\Delta G_v) \quad (4)$$

$$r^*=2\sigma_{\gamma\alpha}/\Delta G_v \quad (5)$$

The schematic illustration of grain boundary ferrite (GBF) nucleation is shown in Figure 12. The calculation equations are shown in eqs (6) and (7).

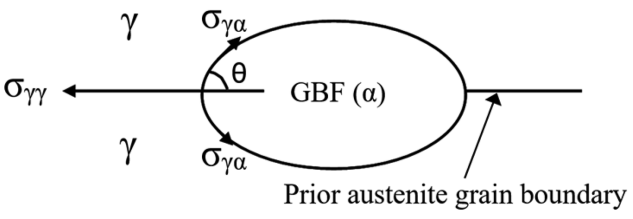

Figure 12: Schematic illustration of ferrite nucleation from prior austenite grain boundary (PAGB) [10].

$$f'(\theta) = \frac{\Delta G^*_{het}}{\Delta G^*_{hom}} = \frac{1}{4}(2+\cos\phi)(1-\cos\phi)^2 \quad (6)$$

$$\cos\phi = \sigma_{\gamma\gamma}/2\sigma_{\gamma\alpha} \quad (7)$$

where $\sigma_{\gamma\gamma}$ is the interfacial energy of austenitic interfaces and cos φ is calculated based on the ratio of $\sigma_{\gamma\gamma}/\sigma_{\gamma\alpha}$.

Figure 13 shows the function between normalized energy barrier of IGF nucleation ($\Delta G^*_{het.}/\Delta G^*_{hom}$) and inclusion size. The chemical parts of the interfacial energies between nucleation sites, which are TiO, TiN and VN, and austenite/ferrite were taken from Refs [42, 53, 75]. The results are shown in Table 2. Also, the interfacial energies between austenite and ferrite which selected were taken from Refs [73, 76, 77]. The results are shown in Table 3. The details of the calculation process and the selection method of interfacial energies are reported in Ref.

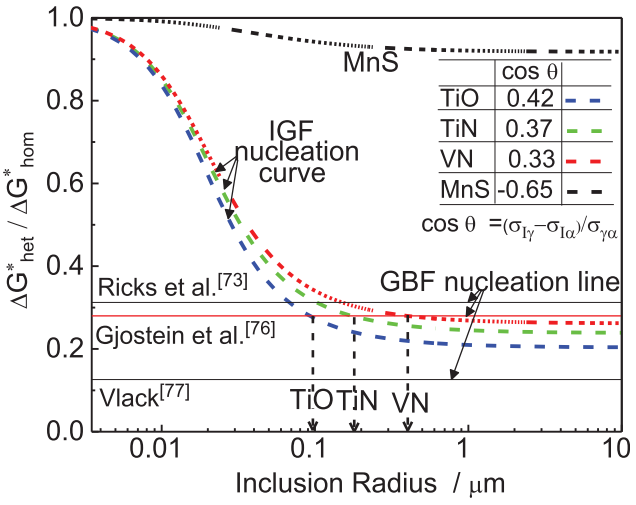

Figure 13: Calculated results of the energy barrier of heterogeneous nucleation, corresponding to the value of homogeneous nucleation [10].

Table 2: Chemical part interfacial energies between the inclusions and austenite/ferrite interfaces, which are used for the calculations of IGF nucleation [10].

Inclusion	$\Delta\sigma = \sigma_{I\gamma} - \sigma_{I\alpha}$ [J/m^2]	$\sigma_{I\gamma}$[J/m^2]	$\sigma_{I\alpha}$[J/m^2]	Ref.
TiN	0.377	1.003	0.626	[75]
	0.197	0.636	0.439	[53]
VN	0.113	0.402	0.289	[75]
	0.326	0.941	0.615	[75]
	0.375	1.595	1.220	[42]
	0.178	0.627	0.449	[53]
TiO	0.226	0.842	0.616	[53]
MnS	−0.35	0.225	0.575	[75]

Table 3: Physical parameters used for the calculation of the grain boundary ferrite nucleation [10].

No.	$\sigma_{\gamma\alpha}/\sigma_{\gamma\gamma}$	Temp.(°C)	Mass.% C in α	Mass.% C in γ	Ref.
1#	0.72	1150	–	–	[77]
2#	0.943	754	0.0175	0.57	[76]
3#	1	–	–	–	[73]

[10]. According to the result in Figure 13, it is seen that the nucleation barrier of IGF decreases with increasing inclusion size, regardless of the inclusion type. Furthermore, the cross point between GBF nucleation barrier line and IGF nucleation barrier curve is regarded as the critical size of nuclei inclusion for IGF. When the inclusion size is larger than the critical size, IGF nucleates instead of GBF since the energy of barrier of IGF nucleation is smaller. It is worth mentioned that the critical diameters of TiO, TiN, and VN inclusions are different. Specifically, it is 0.192 μm for TiO, 0.355 μm for TiN and 0.810 μm for VN. Moreover, this critical values can almost fit the experiment data of minimum effective inclusion size for IGF nucleation using the chemical part of the interfacial energy ($\Delta\sigma = \sigma_{I\gamma} - \sigma_{I\alpha} =$ 0.226 J/m^2 for TiO, 0.197 for TiN and 0.178 for VN), as shown in Figure 9.

The detailed discussion can be seen in Ref. [10]. Besides, the effects of the Mn, C and S contents on the critical size of nuclei inclusion are shown in Figure 14. It is found that the critical size of nuclei inclusion increases with increased manganese or carbon content, since they are austenite stabilizing elements. It is also seen that sulfur does not seem to affect the critical size of TiO, TiN and VN for IGF nucleation. However, increased sulfur content can lead to a larger amount of MnS precipitation. Thus, MnS can cover the surface of the effective nucleation site and decrease the potency of IGF nucleation.

According to the calculation of the critical size of nuclei inclusions using the modified model, the chemical part of the interfacial free energy without physical energy (misfit energy) could be used to obtain the best fit between the experiment data and the calculation results. Specifically, chemical part interfacial energy surely controls the ferrite nucleation from the inclusion surface. Misfit parameter never control it. It is believed to be an important finding to investigate IGF nucleation mechanisms.

Besides TiO, TiN, and VN inclusions, several kinds of spinel inclusions, such as: $MnTi_2O_4$, $MnAl_2O_4$, etc. are also effective nucleation sites for IGF. However, the critical diameters of these spinel inclusions cannot be calculated due to the lack of chemical part of the interfacial

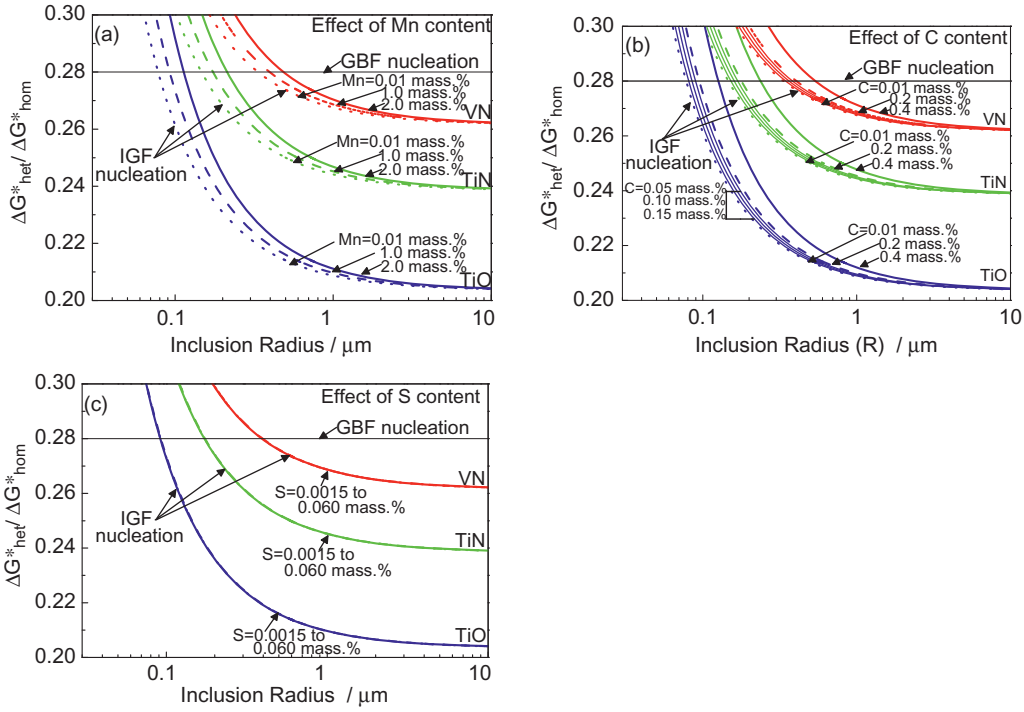

Figure 14: Effects of (a) Mn, (b) C and (c) S contents on the critical sizes of nuclei inclusions for IGF nucleation [10, 13].

energies between inclusion and austenite/ferrite. This should be considered in future work as a complement to the current model study.

Comment on Mn-depleted zone

The Mn-depleted zone (MDZ) is a well-known mechanism to promote IGF formation. Also, MDZ formation occurs either due to that MnS absorbs Mn [78], or due to that Mn replacing Ti in $(Ti,Mn)_2O_3$ [36]. Several studies reported that existence of MDZ promote IGF formation but they only used SEM-EDS to characterize the formation of MDZ. Because the size range of MDZ is very narrow, it is often examined by FE-TEM [78]. In this case, it seems to be very difficult to discuss the existence of MDZ only based on SEM-EDS results.

In situ observations of the IGF formation using confocal laser scanning microscope

The pioneer work to apply high temperature confocal laser scanning microscope (CLSM) in steelmaking is dated back to 1997 from Emi's group [79–81]. Thereafter, this technique has subsequently been used to investigate solidification [79, 80], inclusion agglomeration in liquid steel [81, 82], and phase transformations in solid steels [36, 83–88]. According to the in-situ observation of IGF formation, the pioneer work in the open literatures is dated back to Hanamura, Shibata et al. [83]. After 2005, over 50 papers have been published in the open literatures focusing on different items of kinetic studies of IGF nucleation and growth. The details regarding these papers will not be discussed in the present review, but they will be summarized in the future work by the authors. In recent years, Terasaki and co-workers [36, 86–88] provided quantitative analysis on the effects of Ti and B contents on the IGF formation. SEM-EDS in combination of TEM and auger electron spectroscopy (AES) were used to characterize the nuclei inclusion phase.

In the very recent work by the authors [11, 12], the IGF formation dynamics in the steels with TiN and Ti_2O_3 additions are investigated using CLSM. The typical images of IGF and GBF formation with different magnitude are shown in Figures 15 and 16. By using these images, several items can be quantitatively investigated. For instance, Figure 17 shows the relationship between the prior austenite grain size and the area fraction of IGF. It is found that the fraction of IGF increased with increased grain size. When the grain

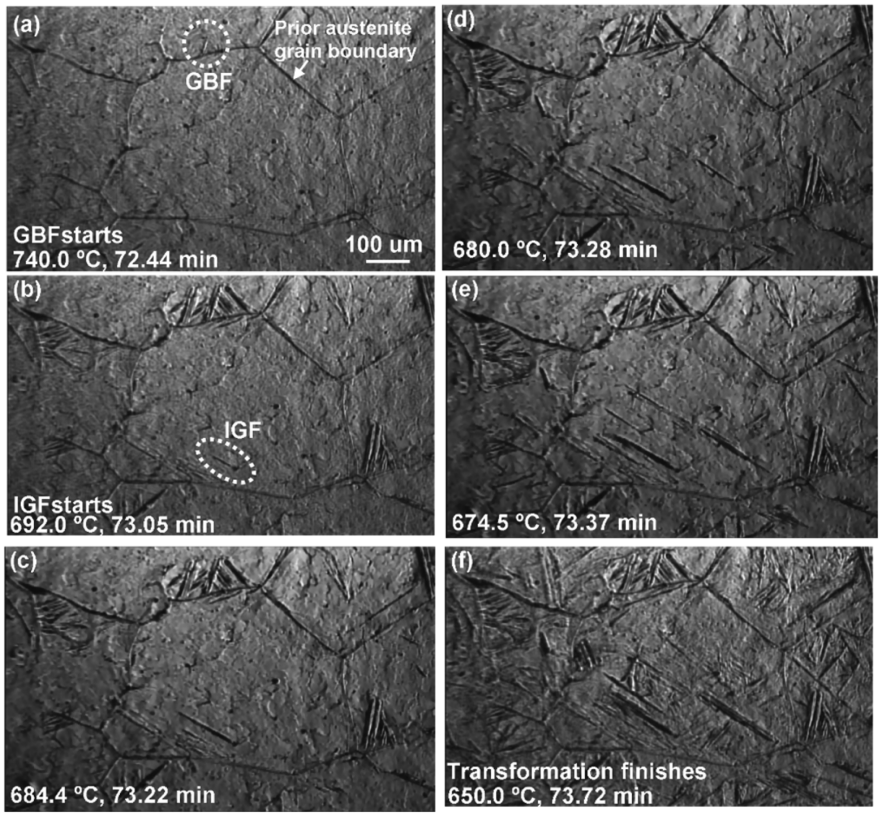

Figure 15: Images observed by confocal laser scanning microscopy (CLSM) for GBF and IGF formation with holding condition of 1400 °C × 0 min and cooling rate of 70 °C/min [10, 11].

size is fixed, it is noted that the fraction of IGF in steel with Ti_2O_3 addition is higher than that of steel with TiN addition. The difference in the fraction of IGF in both cases is due to that TiO_x is more effective to promote IGF formation than TiN [11, 12].

The contributions of in-situ observations of IGF formation by the authors is to quantitatively compare the IGF characteristics including area fraction, starting temperature of IGF and GBF in the steels with TiN and Ti-oxide additions. Moreover, the CLSM measurements in combination with differential scanning calorimetry (DSC) measurements have been used to plot schematic continuous cooling transformation (CCT) diagram of IGF and GBF formation, as shown in Figure 18 [12]. According to the authors' knowledge, this is the first trial to combine these two methodologies to draw CCT diagrams for the austenite decomposition process. In addition, different cooling rates, which are used to simulate the cases of as-cast, welding and quenching, have been quantitatively selected to investigate IGF formation characteristics. For instance, different morphologies of the IGF detected by electron backscatter diffraction (EBSD) are shown in Figure 19 [11]. Till now, the limit of in-situ observations is CLSM can only detect the surface phenomenon. However, the transformation of the steel bulk cannot be observed directly. In future work, the use of the CLSM in combination with in-situ characterization techniques could be used to detect the bulk materials change. Such techniques include x-ray synchrotron tomographic [89] and in situ neutron diffraction [90] are considered to apply, since these techniques have been used to detect in-situ microstructure change of metallic alloys.

Summary

The present work highlights the frontiers of experimental and theoretical investigations of the role of non-metallic inclusions on IGF formations, undertaken by the group of Applied Process Metallurgy, KTH Royal Institute of Technology. The first contribution by the authors is applying the relationship between the inclusion size and IGF nucleation potency to different nucleation sites (TiO_X, TiN, V(C,N)). The results show that different nucleation sites have different effective inclusion sizes for IGF formation. Moreover, a modified IGF nucleation model has been developed. It shows that the chemical

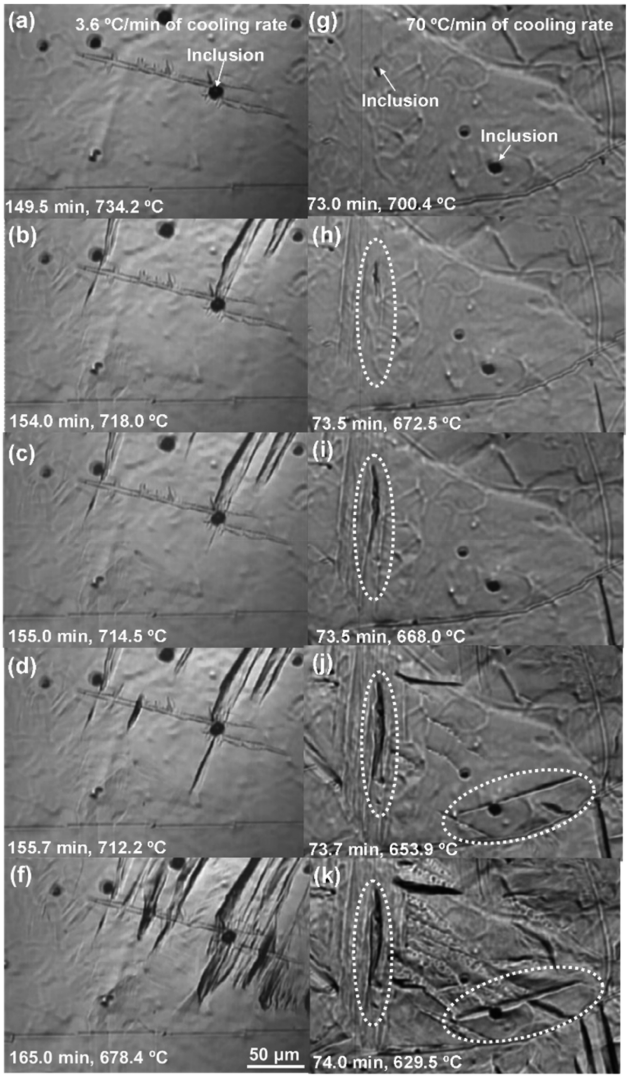

Figure 16: Typical CLSM images for IGF formation in steel with Ti_2O_3 addition, held at 1400 °C/min. (a) to (f) cooling rate of 3.6 °C/min, and (g) to (k) cooling rate of 70 °C/min from 950 to 400 °C [11].

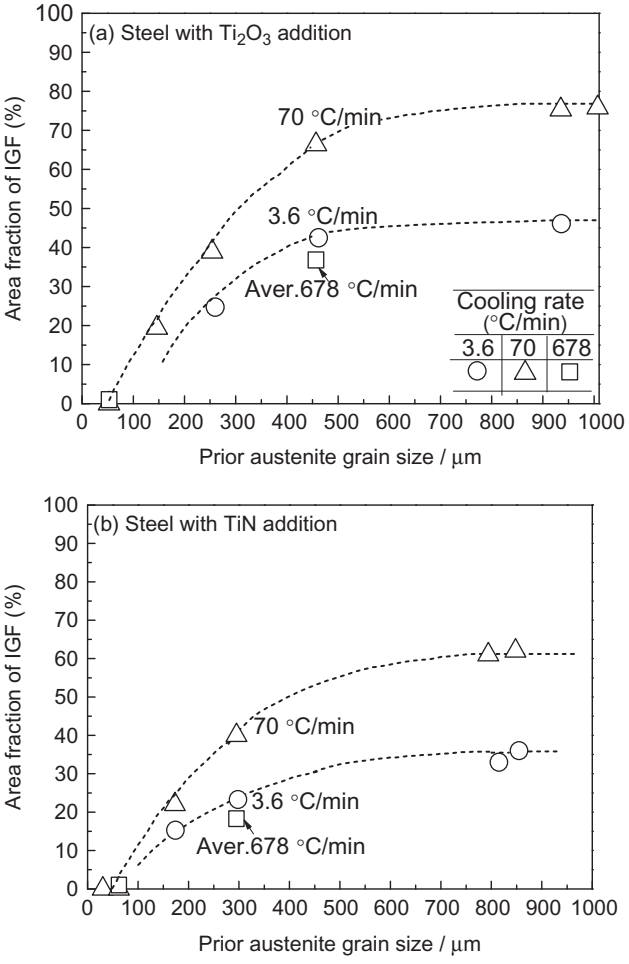

Figure 17: Relationship between the prior austenite grain size and the area fraction of IGF in (a) steel with Ti_2O_3 addition and (b) steel with TiN addition [11].

part interfacial free energy without the misfit energy could lead to a good fit between experiment data and calculation results. In future work, the energy barrier of IGF nucleation from more kinds of nuclei inclusions besides TiO, TiN and VN will be considered by calculating the chemical part interfacial energies between more kinds of inclusions and austenite/ferrite. In addition, the interface between nuclei inclusion and IGF should be highly focused in experimental studies. This requires the development of characterization methodologies such as: high-resolution transmission electron microscopy (HRTEM) with electron energy loss spectroscopy (EELS) or focused ion beam (FIB), and atom probe tomography (APT). It is foreseen that "oxide metallurgy" concept can be applied to other steel grades, such as stainless steel, special steels including nitriding steel in the future.

Acknowledgment: The authors would like to thank Professor Hiroyuki Shibata (IMRAM, Tohoku University) for the support and discussions related to in-situ observations of IGF formations using the CLSM technique. Assistant Professor Peter Hedström (KTH) is acknowledged for valuable discussion, experiment support and good suggestion related to austenite decomposition. Dr. Huahai Mao (KTH) is acknowledged for the support and discussions of thermodynamic calculations by using Thermo-Calc. software. W.M. is also grateful to the China Scholarship Council (CSC) and JASSO Scholarship foundation for the financial support to carry out his research at KTH Royal Institute of Technology and at Tohoku University.

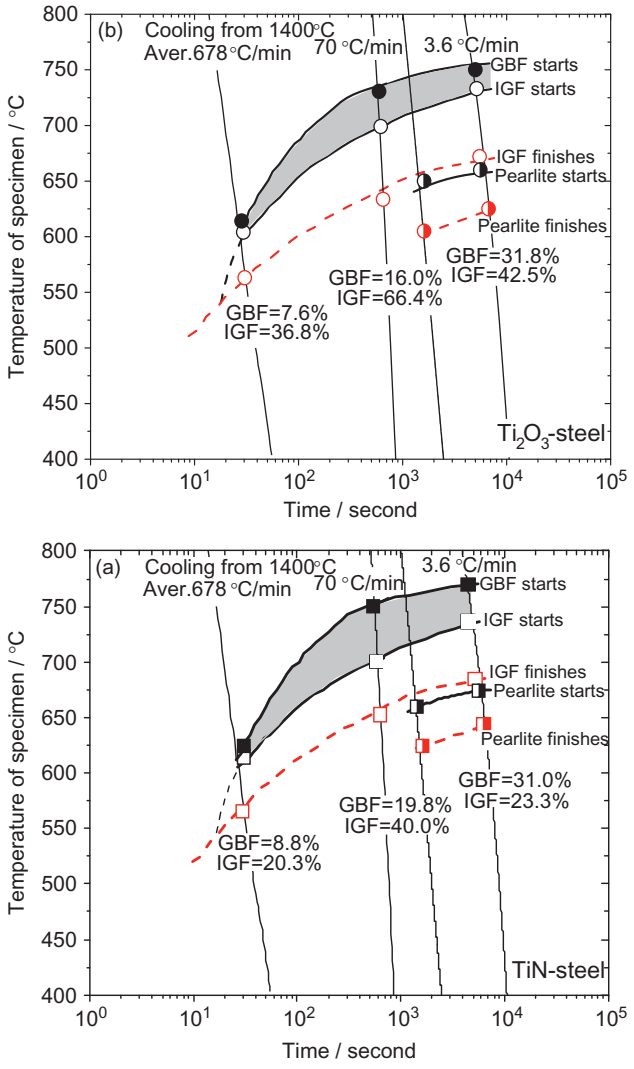

Figure 18: Schematic CCT diagram of austenite decomposition for (a) steel with Ti_2O_3 addition and (b) steel with TiN addition [12].

Reference

[1] J. Takamura and S. Mizoguchi, Proceedings of 6th International Iron and Steel Congress, ISIJ, Nagoya, Japan (1990), Vol. I, pp. 591–597.

[2] S. Mizoguchi and J. Takamura, Proceedings of 6th International Iron and Steel Congress, ISIJ, Nagoya, Japan (1990), Vol. I, pp. 598–604.

[3] T. Sawai, M. Wakoh, Y. Ueshima and S. Mizoguchi, Proceedings of 6th International Iron and Steel Congress, ISIJ, Nagoya, Japan (1990), Vol. I, pp. 605–611.

[4] S. Ogibayashi, K. Yamaguchi, M. Hirai and H. Goto, Proceedings of 6th International Iron and Steel Congress, ISIJ, Nagoya, Japan (1990), Vol. I, pp. 612–617.

[5] S.S. Babu, Curr. Opin. Solid State Mater. Sci., 8 (2004) 267–278.

[6] T. Koseki and G. Thewlis, Mater. Sci. Technol., 21 (2005) 867–879.

[7] D.S. Sarma, A.V. Karasev and P.G. Jönsson, ISIJ Int., 49 (2009) 1063–1074.

[8] W. Mu, P.G. Jönsson, H. Shibata and K. Nakajima, Steel Res. Int., 87 (2016) 339–348.

[9] W. Mu, P.G. Jönsson and K. Nakajima, ISIJ Int., 54 (2014) 2907–2916.

[10] W. Mu, P.G. Jönsson and K. Nakajima, J. Mater. Sci., 51 (2016) 2168–2180.

[11] W. Mu, H. Shibata, P. Hedström, P.G. Jönsson and K. Nakajima, Metall. Mater. Trans. B, 47B (2016) 2133–2147.

[12] W. Mu, H. Shibata, P. Hedström, P.G. Jönsson and K. Nakajima, Steel Res. Int., 87 (2016) 10–16.

[13] W. Mu, H. Mao, P.G. Jönsson and K. Nakajima, Steel Res. Int., 87 (2016) 311–319.

[14] C. Xuan, W. Mu, Z.I. Olano, P.G. Jönsson and K. Nakajima, Steel Res. Int., 87 (2016) 911–920.

[15] W. Mu, P.G. Jönsson and K. Nakajima, 6th International Congress on the Science and Technology of Steelmaking (ICS2015), Beijing, China (2015), Vol. II, pp. 767–771.

[16] W. Mu, P.G. Jönsson and K. Nakajima, Challenges and Transformative Solutions to Sustainable Steelmaking and

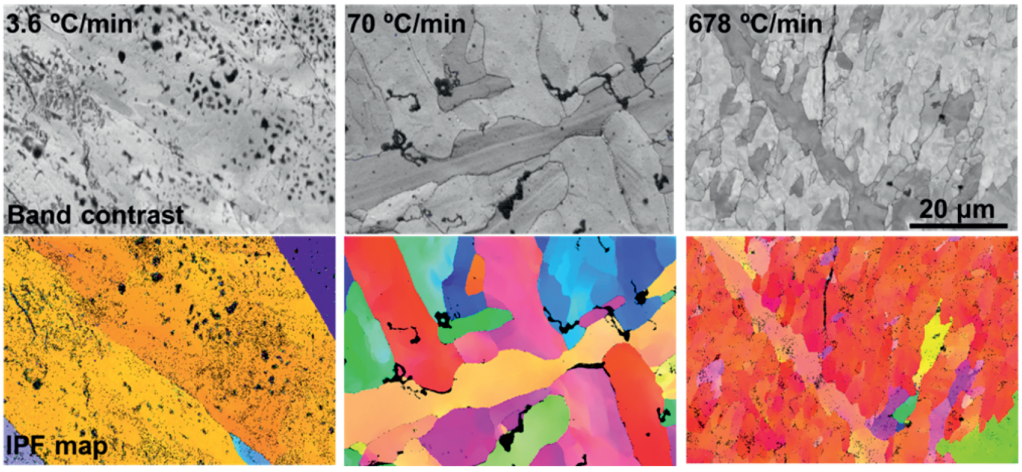

Figure 19: EBSD analysis of steel with Ti_2O_3 addition at different cooling rates [11].

Casting for Environment-Friendly Metallurgical Innovation (CTSSC-EMI, Emi Symposium), Tokyo, Japan (2015), pp. 64–71.
[17] J.M. Gregg and H.K.D.H. Bhadeshia, Metall. Mater. Trans. A, 25A (1994) 1603–1611.
[18] S. Zhang, N. Hattori, M. Enomoto and T. Tarui, ISIJ Int., 36 (1996) 1301.
[19] K. Kasai, C. Lee, S. Nambu, J. Inoue and T. Koseki, Tetsu-to-Hagané, 96 (2010) 123–128.
[20] C. Lee, S. Nambu, J. Inoue and T. Koseki, ISIJ Int., 51 (2011) 2036–2041.
[21] J.M. Gregg and H.K.D.H. Bhadeshia, Acta Mater., 43 (1997) 739–748.
[22] Ø. Grong, L. Kolbeinsen, C. van der Eijk and G. Tranell, ISIJ Int., 46 (2006) 824–831.
[23] M. Kiviö, L. Holappa and T. Iung, Metall. Mater. Trans. B, 41B (2010) 1194–1204.
[24] X. Gao, S. Yang, J. Li, H. Liao, W. Gao and T. Wu, Metall. Mater. Trans. B, 47B (2016) 1124–1136.
[25] H. Homma, S. Ohkita, S. Matsuda and K. Yamamoto, Welding J., 66 (1987) 301–305.
[26] R. Chijiwa, H. Tamehiro, M. Hirai, H. Matsuda and H. Mimura, Proceedings of the 7th International Conference on Offshore Mechanics and Arctic Engineering (OMAE 88), ASME, Houston, Texas (1988), Vol. V, pp. 165–172.
[27] J.-S. Byun, J.-H. Shim, Y.W. Cho and D.N. Lee, Acta Mater., 51 (2003) 1593–1606.
[28] T. Suzuki, J. Inoue and T. Koseki, Proceedings of the 8th International Conference on Trends in Welding Research, ASM Int., Pine Mountain, Georgia (2009), pp. 292.
[29] T. Ichinose, H. Okaguchi and Y. Komizo, Camp-Isij, 11 (1998) 531.
[30] T. Ichinose, H. Okaguchi and Y. Komizo, Camp-Isij, 12 (1999) 533.
[31] S. Kanazawa, A. Nakashima, K. Okamoto and K. Kanaya, Tetsu-to-Hagané, 61 (1975) 2589–2603.
[32] S. Matsuda and H. Kageyama, Tetsu-to-Hagané, 62 (1976) 1356–1362.
[33] Y. Morikage, K. Oi, F. Kawabata and K. Amano, Tetsu-to-Hagané, 84 (1998) 510–515.
[34] J.-H. Shim, Y.-J. Oh, J.-Y. Suh, Y.W. Cho, J.-D. Shim, J.-S. Byun and D.N. Lee, Acta Mater., 49 (2001) 2115–2122.
[35] I. Madariaga, J.L. Romero and I. Gutierrez, Metall. Mater. Trans. A, 29 (1998) 1003–1015.
[36] D. Zhang, H. Terasaki and Y. Komizo, Acta Mater., 58 (2010) 1369–1378.
[37] Y. Tomita, N. Saito, T. Tsuzuki, Y. Tokunaga and K. Okamoto, ISIJ Int., 34 (1994) 829–835.
[38] C. Van Der Eijk, Ö. Grong and J. Hjelen, Proceedings of an International Conference on Solid-solid Phase Transformations, JIM, Sendai (1999), pp. 1573–1576.
[39] H.H. Jin, J.H. Shim, Y.W. Cho and H.C. Lee, ISIJ Int., 43 (2003) 1111–1113.
[40] K. Yamamoto, T. Hasegawa and J. Takamura, Tetsu-to-Hagané, 79 (1993) 1169.
[41] Y. Ohno, Y. Okamura, S. Matsuda, K. Yamamoto and T. Mukai, Tetsu-to-Hagané, 73 (1987) 1010–1017.
[42] T. Furuhara, J. Yamaguchi, N. Sugita, G. Miyamoto and T. Maki, ISIJ Int., 43 (2003) 1630–1639.
[43] T. Furuhara, T. Shinyoshi, G. Miyamoto, J. Yamaguchi, N. Sugita, N. Kimura, N. Takemura and T. Maki, ISIJ Int., 43 (2003) 2028–2037.
[44] A.M. Guo, S.R. Li, J. Guo, P.H. Li, Q.F. Ding, K.M. Wu and X.L. He, Mater. Charact., 29 (2008) 134–139.
[45] M.H. Shi, P.Y. Zhang and F.X. Zhu, ISIJ Int., 54 (2014) 188–192.
[46] X.L. Wan, K.M. Wu, L. Cheng and R. Wei, ISIJ Int., 55 (2015) 679–685.
[47] C. Wang, R.D.K. Misra, M.H. Shi, P.Y. Zhang, Z.D. Wang, F.X. Zhu and G.D. Wang, Mater. Sci. Eng. A, 594 (2014) 218–228.
[48] M. Jiang, Z.Y. Hu, X.H. Wang and J.J. Pak, ISIJ Int, 53 (2013) 1386–1391.
[49] X. Li, Y. Min, C. Liu and M. Jiang, Steel Res. Int., 86 (2015). DOI:10.1002/srin.201500167.
[50] Y. Li, X.L. Wan, L. Cheng and K.M. Wu, Scripta Mater., 75 (2014) 78–81.
[51] W. Bin and S. Bo, Steel Res. Int., 83 (2012) 487–495.
[52] Y. Min, X. Li, Z. Yu and M. Jiang, Steel Res. Int., 87 (2016). DOI:10.1002/srin.201500440.
[53] Z. Yang, C. Zhang and T. Pan, Mater Sci Forum, 475–479 (2005) 113–116.
[54] J. Hu, L.X. Du and J.J. Wang, Scripta Mater., 68 (2013) 953–956.
[55] F. Ji, C. Li, S. Tang, G. Yuan and G. Wang, ISIJ Int., 56 (2016) 602–609.
[56] M. Kapoor, R. O'Malley and G.B. Thompson, Metall. Mater. Trans. A, 47A (2016) 1984–1995.
[57] S.V. Subramanian, X. Ma, W. Nie and X. Zhang, Proceedings of HSLA Steels 2015, Microalloying 2015 & Offshore Engineering Steels 2015, TMS, Hangzhou, China, pp. 211–221.
[58] X. Li, D. Wang, C. Liu and M. Jiang, J. Northeastern Univ., 35 (2014) 529–533. DOI:10.3969/j.issn.1005-3026.
[59] TCS Steels/Fe-Alloys Database Version 7.0, Thermo-Calc Software AB, Sweden (2012).
[60] S. St-Laurent and G. L'Espérance, Mater. Sci. Eng. A, 149 (1992) 203–216.
[61] Z. Zhang and R.A. Farrar, Mater. Sci. Technol., 12 (1996) 237–260.
[62] K.F.A. Hajeri, C.I. Garcia, M. Hua and A.J. Deardo, ISIJ Int., 46 (2006) 1233–1240.
[63] T.K. Lee, H.J. Kim, B.Y. Kang and S.K. Hwang, ISIJ Int., 40 (2000) 1260–1268.
[64] Y. Oh, S. Lee, J. Byun, J. Shim and Y. Cho, Mater. Trans., JIM, 41 (2000) 1663–1669.
[65] B. Kim, S. Uhm, C. Lee, J. Lee and Y. An, J. Eng. Mater. Technol., 127 (2005) 204–213.
[66] N. Kikuchi, S. Nabeshima, Y. Kishimoto, T. Matsushita and S. Sridhar, ISIJ Int., 47 (2007) 1255–1264.
[67] N. Kikuchi, S. Nabeshima, Y. Kishimoto and S. Sridhar, ISIJ Int., 48 (2008) 934–943.
[68] N. Kikuchi, S. Nabeshima, Y. Kishimoto, Y. Ishiguro and S. Sridhar, ISIJ Int., 49 (2009) 1036–1045.
[69] N. Kikuchi, S. Nabeshima, T. Yamashita, Y. Kishimoto, S. Sridhar and T. Nagasaka, ISIJ Int., 51 (2011) 2019–2028.
[70] N.H. Fletcher, J. Chem. Phys., 29 (1958) 572–576.
[71] H. Vehkamäki, A. Määtänen, A. Lauri and M. Kulmala, Atoms. Chem. Phys., 7 (2007) 303–313.
[72] K.F. Kelton and A.L. Greer, Nucleation in Condensed Matter – Application in Materials and Biology, Elsevier, Oxford, UK (2010), pp. 51–52, 182–184.
[73] R. Ricks, P.R. Howell and G.S. Barritte, J. Mater. Sci., 17 (1982) 732–740.
[74] J.S. Byun, J.H. Shim, Y.W. Cho and D.N. Lee, Acta Mater., 51 (2003) 1593–1606.

[75] Use of Fine Inclusions in Microstructure Control of Steels, Final report of fine inclusions committee, the Iron and Steel Institute of Japan (1995), pp. 75.
[76] N.A. Gjostein, H.A. Domian, H.I. Aaronson and E. Eichen, Acta Metall., 14 (1966) 1637–1644.
[77] L.H. Van Vlack, Trans. A.I.M.E., 191 (1951) 251–259.
[78] H. Mabuchi, R. Uemori and M. Fujioka, ISIJ Int., 36 (1996) 1406–1412.
[79] H. Chikama, H. Shibata, T. Emi and M. Suzuki, Mater. Trans., JIM, 37 (1996) 620–626.
[80] H. Shibata, H.B. Yin, S. Yoshinaga, T. Emi and M. Suzuki, ISIJ Int., 38 (1998) 149–156.
[81] H.B. Yin, H. Shibata, T. Emi and M. Suzuki, ISIJ Int., 37 (1997) 936–945.
[82] K. Nakajima and S. Mizoguchi, Metall. Mater. Trans. B, 32 (2001) 629–641.
[83] T. Hanamura, H. Shibata, Y. Waseda, H. Nakajima, S. Torizuka, T. Takanashi and K. Nagai, ISIJ Int., 39 (1999) 1188–1193.
[84] X. Wan, K. Wu, G. Huang and R. Wei, Steel Res. Int., 85 (2014) 243–250.
[85] X.L. Wan, K.M. Wu, L. Cheng and R. Wei, ISIJ Int., 55 (2015) 679–685.
[86] H. Terasaki, T. Yamada and Y. Komizo, Mater. Sci. Forum, 580–582 (2008) 33–36.
[87] T. Yamada, H. Terasaki and Y. Komizo, Weld. Int., 23 (2009) 376–381.
[88] D. Zhang, Y. Shintaku, S. Suzuki and Y. Komizo, Metall. Mater. Trans. A, 43A (2012) 447–458.
[89] B. Cai, J. Wang, A. Kao, K. Pericleous, A.B. Phillion, R.C. Atwood and P.D. Lee, Acta Mater., 117 (2016) 160–169.
[90] A. Lombardi, D. Sediako, C. Ravindran and R. MacKay, Can. Metall. Q., 54 (2015) 30–37.